

Decoding disorder signatures of AuCl_3 and vacancies in MoS_2 films: from synthetic to experimental inversion

F R Duarte^{1,*} , F Matusalem^{2,3} , D Grasseschi⁴ , A R Rocha² , Leandro Seixas^{5,6} , Christiano J S de Matos^{5,6}, S Mukim¹  and M S Ferreira^{1,7} 

¹ School of Physics, Trinity College Dublin, Dublin 2, Ireland

² Instituto de Física Teórica (IFT), Universidade Estadual Paulista (UNESP), Rua Dr Bento T. Ferraz, 271, São Paulo 01140-070, Brazil

³ Grupo de materiais semicondutores e nanotecnologia (GMSN), Instituto Tecnológico de Aeronáutica (ITA), 12228-900 São José dos Campos/SP, Brasil

⁴ Inorganic Chemistry Department, Chemistry Institute, Federal University of Rio de Janeiro, Rio de Janeiro, Brazil

⁵ School of Engineering, Mackenzie Presbyterian University, Rua da Consolação 930, São Paulo SP 01302-907, Brazil

⁶ MackGraphe—Mackenzie Institute for Research in Graphene and Nanotechnologies, Mackenzie Presbyterian Institute, Rua da Consolação 930, São Paulo SP 01302-907, Brazil

⁷ Centre for Research on Adaptive Nanostructures and Nanodevices (CRANN) & Advanced Materials and Bioengineering Research (AMBER) Centre, Trinity College Dublin, Dublin 2, Ireland

E-mail: duarteff@tcd.ie

Received 5 June 2024, revised 16 August 2024

Accepted for publication 28 August 2024

Published 6 September 2024



CrossMark

Abstract

This study investigates the scope of application of a recently designed inversion methodology that is capable of obtaining structural information about disordered systems through the analysis of their conductivity response signals. Here we demonstrate that inversion tools of this type are capable of sensing the presence of disorderly distributed defects and impurities even in the case where the scattering properties of the device are only weakly affected. This is done by inverting the DC conductivity response of monolayered MoS_2 films containing a minute amount of AuCl_3 coordinated complexes. Remarkably, we have successfully extracted detailed information about the concentration of AuCl_3 by decoding its signatures on the transport features of simulated devices. In addition to the case of theoretically generated Hamiltonians, we have also carried out a full inversion procedure from experimentally measured signals of similar structures. Based on experimental input signals of MoS_2 with naturally occurring vacancies, we were able to quantify the vacancy concentration contained in the samples, which indicates that the inversion methodology has experimental applicability as long as the input signal is able to resolve the characteristic contributions of the type of disorder in question. Being able to handle more complex, realistic scenarios unlocks the method's applicability for designing and engineering even more elaborate materials.

* Author to whom any correspondence should be addressed.



Original Content from this work may be used under the terms of the [Creative Commons Attribution 4.0 licence](https://creativecommons.org/licenses/by/4.0/). Any further distribution of this work must maintain attribution to the author(s) and the title of the work, journal citation and DOI.

Keywords: theoretical, transition metal dichalcogenides, monolayer MoS₂, coordinated complexes, inversion, KITE

1. Introduction

Research on bidimensional materials design, especially involving 2D transition metal dichalcogenides (TMDs), has been in focus since the last decade for their characteristic thermal, mechanical, and electronic properties [1–9]. Along with it, methods for enhancing their properties, such as chemical functionalization, are of immense interest and are driven by the possibility of tuning their electronic, optical, and catalytic capabilities [10–18]. Such doping techniques rely on the fabrication of lattice defects; that is, they rely on systematic breakage of the crystalline symmetry through vacancies, chemical adsorptions, or atom substitutions, to mention but a few [19–24]. These defects modify the transport properties of materials but have the drawback of drastically elevating the complexity of any attempt to theoretically describe and accurately predict their detailed responses to externally applied fields.

For example, it is well established that adding non-periodic inclusions to an otherwise crystalline system will always make *ab initio* calculations significantly more costly. For the same reason, once disorder comes into play, even greater becomes the cost for solving the inverse problem, i.e. the recovery of the system's composition from its spectral measurements. Driven by the ultimate goal of designing materials that behave on our own accord, we must be able to accurately determine the effect that the concentration of a given set of defects has on the properties of a system. Consequently, finding the solution to such inverse problems is paramount.

One approach for designing a material with a specific measurement response is determining what configuration of elements and impurities a system needs to generate a desired signal. This is normally referred to as an inverse problem, and by definition, problems of that type are convoluted by nature. Similarly to the endeavor of determining an object from its shadow projected on a wall, this problem consists of determining the components of a system from a measurement of one of its spectral function projections on the space of a significant quantity. An inversion method capable of decoding any signature in this way has to be able to accurately detect the presence and quantity of different types of disorder in the system. To make matters worse, defects and impurities often have very distinct signatures on how they impact a system's response. While substitutional impurities are expected to have a stronger impact on the transport properties, adsorbed atoms and molecules or coordinated complexes tend to cause weaker changes to the transport features. Being able to extract structural information from a system composed of substitutional and adsorbed impurities can be seen as a way to attest to the sensitivity of one's inversion procedure.

With that in mind, we apply a recently formulated methodology capable of extracting the information about the number of impurities on various systems based on the minimization of a functional that draws out information from a measurement signature [25–28]. This inversion method has demonstrated reliable accuracy when applied to a variety of systems and input quantities. The method has been successfully implemented to acquire information regarding vacancies as well as multiple substitutional impurities in various different materials. Furthermore, the method has been used to obtain information not only of global quantities, e.g. the total impurity concentration, but also information of a local nature such as the spatial mapping of the underlying disorder [27]. However, all cases studied thus far have involved fully synthetic cases in which a Hamiltonian associated with a disordered configuration is employed to generate the physical response of that specific system. Using this response as the sole input of the methodology, the inversion task consists of obtaining as much information as possible about that specific Hamiltonian without availing of any prior knowledge about that synthetically generated system. Such a synthetic case is supposed to serve as a proxy for the realistic situation of using experimentally obtained signals as the inversion input function.

In this article, we further expand the aforementioned inversion methodology by applying it to a novel, more complex system—thin films of molybdenum disulfide (MoS₂) with adsorbed gold coordination complexes (AuCl₃) in the presence of vacancies. Besides testing the accuracy of the inversion method with coexisting substitutional and adsorbed impurities, we also consider the case of experimentally generated signals as the sole input function, in addition to the usual synthetic approach.

Different chemical functionalization techniques have been carried out on MoS₂ such as organohalides functionalization on liquid exfoliated flakes [29, 30], functionalization on MoS₂ grown by chemical vapor deposition with ligands that passivate the chalcogen vacancies [14, 31] and the recently developed route of single Au atoms functionalization via the formation of S-Au-Cl₃ coordination complexes, which allow for Fermi level tuning via p-type doping, high exciton-to-trion ratios on the photoluminescence spectrum and enhanced thermal boundary conductance [16]. The latter comprises a kind of functionalization that does not depend on the presence of lattice defects for passivation or substitution, so we can straightforwardly model it using a combination of Density Functional Theory (DFT) and Tight Binding (TB) techniques [32–35]. The independence between the occupancy of S-Au-Cl₃ complexes and the presence of S vacancies further allows for an uncomplicated combination of both types of disorder in our simulations. Since the chalcogen vacancies are commonly

formed defects due to the types of atomic bonding in mono-layer TMDs [36–40], it is essential that such defects are considered during simulations and while designing materials with TMD as hosts. That justifies our choice of host and dopant since the adsorbed AuCl_3 coexist with vacancies, which ultimately are equivalent to substitutional impurities.

2. Methods

2.1. Theoretical calculations

The inversion method in question consists of minimizing the functional $\chi(n)$ that computes the misfit between a measurement signal and the calculated average of that response over different configurations containing disorder in a concentration n given by

$$\chi(n) = \frac{1}{\varepsilon_+ - \varepsilon_-} \int_{\varepsilon_-}^{\varepsilon_+} dE [\Gamma(E) - \langle \Gamma(E, n) \rangle]^2, \quad (1)$$

where $\Gamma(E)$ is the input signal of choice evaluated at energy E . To avoid the ill-definition of the inversion problem, we assume such an input signal belongs to a definite system containing an unknown amount of disorder. Alternatively, we can interpret this as the signal we want to mimic by implementing the appropriate amount of disorder to the pristine defined system. One obtains such correct concentration n_{\min} by minimizing the functional $\chi(n)$. ε_{\pm} are the extremity values of the selected energy spectrum range, and $\langle \Gamma(E, n) \rangle$ is the Configuration Average (CA) of that quantity over N_c configurations containing a concentration of disorder n calculated as [26]

$$\langle \Gamma(E, n) \rangle = \frac{1}{N_c} \sum_{m=1}^{N_c} \Gamma_m(E, n). \quad (2)$$

The function $\Gamma_m(E, n)$ on the righthand side of equation (2) is then calculated from a TB model for the different configurations considered. The TB Hamiltonian, in turn, is generated with parameters obtained from DFT calculations. Here, we considered two situations, pristine monolayer MoS_2 , and a AuCl_3 complex adsorbed on the TMD chalcogen. The primitive 2D MoS_2 unit cell has hexagonal symmetry and is formed by a triple atomic layer with the Mo layer sandwiched by two S ones [41]. For our calculations, we use a rectangular cell replicated 3×4 times (36 atoms), forming a supercell with dimensions $9.77 \text{ \AA} \times 11.28 \text{ \AA}$ and with 3.22 \AA of thickness after the DFT relaxation process. To avoid spurious interactions between mirror cells along the normal to the plane direction, 15 \AA of vacuum is included. For the AuCl_3 -adsorbed case, one AuCl_3 complex was included with the gold atom positioned 2.69 \AA (after relaxation) above a S atom, as shown in figure 1(a). The total-energy and electronic-structure results were obtained via DFT as implemented in the SIESTA code [42]. Exchange and correlation are described by a combination of a revised version of the Perdew-Wang 86 (rPW86) [43] exchange functional, with a semilocal correlation energy functional in the generalized gradient approximation of Perdew, Burke, and Ernzerhof (PBE) [44] and a nonlocal van der Waals

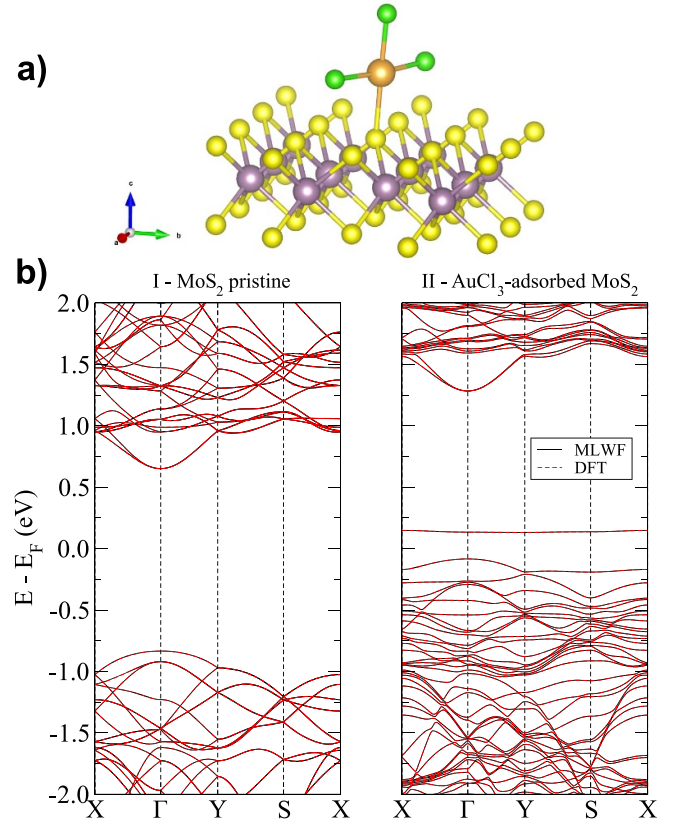


Figure 1. (a) Standard orientation of crystal shape for the $(\text{MoS}_2)\text{AuCl}_3$ disorder unit cell (purple sphere = Mo, yellow sphere = S, gold sphere = Au, green sphere = Cl). (b) Electronic band structure of **I** - pristine MoS_2 and **II** - AuCl_3 -adsorbed MoS_2 calculated via DFT (red dashed lines) and the corresponding MLWF one (black solid lines). The agreement between the curves is such that it makes them hardly distinguishable.

contribution proposed by Vydrov *et al* [45]. The inclusion of van der Waals corrections is important in this case to correctly describe the interaction between the adsorbed molecule and the monolayer MoS_2 [46]. A double- ζ -polarized (DZP) basis set with a real-space grid cutoff of 200 Ry is used. The BZ is sampled using a $6 \times 6 \times 1$ Monkhorst–Pack k-point mesh.

To obtain the TB parameters from the DFT results, we employed the Maximally localized Wannier functions (MLWF) method [47, 48] as implemented in the Wannier90 code [49]. We considered the projections of p_x, p_y and p_z orbitals of the chalcogen atoms and the five d orbitals of Mo, as well as the s and all the p orbitals of Au and Cl, respectively. The disentanglement procedure reached a convergence of the order of 10^{-8} , resulting in a very good agreement of the MLWF bands in comparison with the DFT ones, as can be viewed in figure 1(b). Experimental results for MoS_2 , fabricated in its single layer form, by means of mechanical exfoliation, exhibit a direct band gap of 1.8–1.9 eV [50]. We found a direct band gap of 1.5 eV for monolayer MoS_2 , which is a slightly lower value. However, G0W0 corrections overestimate the band gap to 2.6–2.7 eV [51]. In such a scenario we chose to keep the PBE result.

To tackle the memory and computational costs of calculating the configurational averages, we solve Kubo's formulas for DC conductivity using the Chebyshev polynomials Green function method via the quantum transport software for real space TB simulations KITE [52–54], where we can set the simulated temperature at $T = 300$ K by altering the modulating Fermi–Dirac distribution. Once we are dealing with large lattices with no translational symmetry due to defects, this real-space high-performance software proves exceptionally useful for performing spectral calculations. The DFT-derived parameters corresponding to a pristine MoS₂ unit cell (all the onsite potentials for each orbital as well as all the second-nearest-neighbors inter-orbital hoppings of the 3×4 set of primitive MoS₂ cells) serve to establish the repetition base for a pristine description of the MoS₂ system. This unit cell comprises 132 orbitals—three **p** orbitals for each sulfur atom and five **d** orbitals for each molybdenum atom. In addition, ten more empty, disconnected orbitals are reserved in the modelling of the unit cell to later house the adsorbed impurities in case the given unit cell is selected to have such an impurity. Now, we use the DFT-derived TB parameters relative to the unit cell containing 3×4 MoS₂ cells plus one coordinated AuCl₃ complex composed by one **s** orbital for gold and three **p** orbitals for each chlorine that define the orbitals of the adsorbed impurity in our model (illustrated in figure 1(a)). In accordance with the disorder concentration value, unit cells containing impurities will replace various random 3×4 sites in our lattice with new orbital and inter-orbital parameters for the Mo and S atoms altered with relation to the pristine case. In this case, the energies and connections relative to the impurity atoms replace the orbitals previously held as empty, disconnected mock orbitals in our modelling. The unit cells are repeated to form 54 067 nm² systems with randomly placed impurities in different sites with predetermined concentrations. Our built systems comprise approximately $7.1 \cdot 10^6$ orbitals on a 64×64 unit cell grid containing various disorder concentrations. In each DC conductivity calculation, we used an expansion of 2048 moments of the Chebyshev polynomials for 3 different random trace vector iterations [55].

Figure 2 shows the effect of AuCl₃ complexes and vacancies on the band gap. The vacancies are simulated by imposing a high onsite potential in the target orbitals—here the **s** and **p** orbitals of various S atoms in the 3×4 reproduction cell. The very occurrence of the unique peaks produced by the presence of disorder illustrates how the CAs with different disorder concentrations provide unique curves that populate the space of possible input signals. Here, the concentration of AuCl₃ is exaggerated to make the peaks visible on the same scale. The positions of the peaks indicate an independence between the types of disorder in the transmission gap region. Such effective orthogonality within the disorder concentration range of interest guarantees that AuCl₃ inversions and vacancy inversions can be performed separately, minimizing the overall cost of the inversion procedure from scaling exponentially with the number of disorder types to linearly in this case.

Since we aim to carry out inversion tasks not only from synthetically generated signals but also from experimentally measured ones, in what follows we include a brief

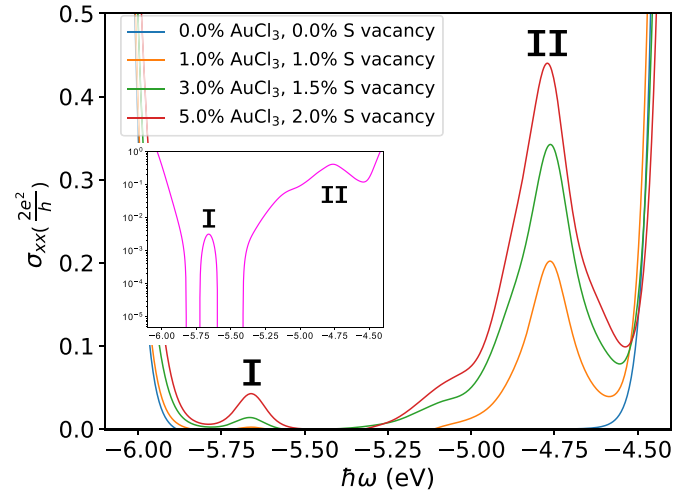


Figure 2. Intra-gap effect of the disorders shown in averages over 40 configurations. The heights of the peaks **I** are proportional to the increased presence of AuCl₃. The concentrations of AuCl₃ are exaggerated to illustrate both peaks in the same scale. The heights of the peaks **II** are proportional to the increased presence of S vacancies. In the inset, we can see the case for typical concentrations of 1% AuCl₃ and 2% S vacancies in the purple log-linear plot.

account of the experimental details of the material fabrication. Subsequent information about the conductivity measurements will also be provided.

2.2. Material fabrication

MoS₂ flakes were synthesized on 300 nm thick SiO₂/Si substrates using the chemical vapor deposition (CVD) method as in the previous work [16]. Here, MoO₃ (6mg) and NaCl (24 mg) powders were mixed and placed in an alumina boat in the high-temperature zone of the CVD furnace. The substrate was placed facedown above the alumina boat containing the NaCl/MoO₃ mixture. Meanwhile, 140 mg of pure sulfur was placed in another alumina boat in a low-temperature zone. Both alumina boats were placed at a distance of 22 cm along the quartz tube furnace. First, a flow rate of 600 sccm of high-purity argon (Ar) gas was passed through the experimental setup for 15 min to purge the quartz tube. Subsequently, a flow rate of 200 sccm (Ar) was maintained during the growth process. The Sulphur temperature was 250 °C. The growth temperature to obtain MoS₂ monolayers was $T = 850$ °C (high-temperature zone) for 10 min and after that, the system was cooled down.

Monolayer MoS₂ flakes morphological characterization was performed by optical and atomic force microscopies. AFM measurements were performed using an NT-MDT Solver Next microscope equipped with feedback sensors, ensuring a Noise XY of less than 0.3 nm and a Noise level Z (RMS in the band of 10–1000 Hz) typically at 0.03 nm. Non-contact mode imaging was employed, utilizing a Force Modulation AFM Probe featuring a Platinum Overall Coating, a force constant of 3 N m^{-1} , resonance frequency of 75 kHz, and dimensions of 225 μm length and 28 μm width. The

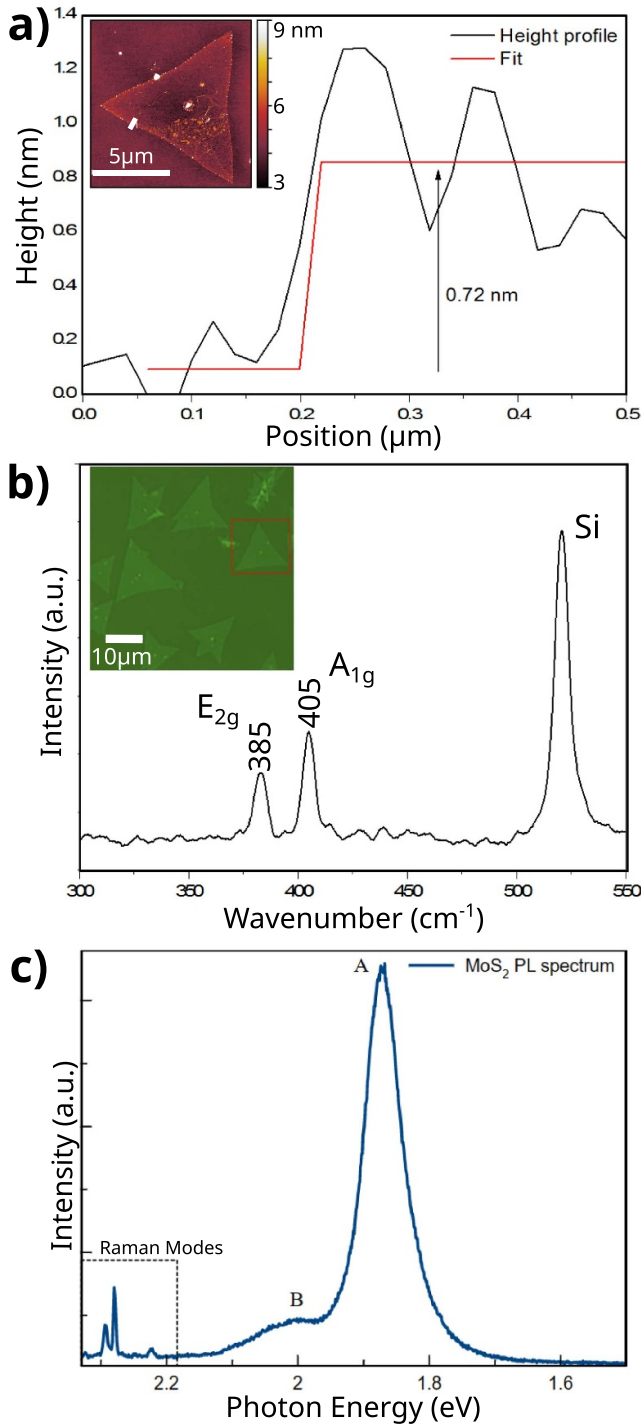


Figure 3. Characterization of monolayer MoS₂. (a) AFM height profile and topographic image (inset). (b) Optical image (inset) and Raman spectrum. (c) Photoluminescence spectrum.

formation of triangle-shaped nanocrystals with a mean lateral dimension of approximately 20 μm is observed (inset in figures 3(a) and (b)). The thickness of these triangular crystals determined by the height profile of AFM measurements (figure 3(a)) is around 0.7 nm, confirming the formation of monolayers. The Raman spectra (figure 3(b)) also confirm the flake's monolayer nature by the presence of two Raman-active

modes at the Γ point: E_{2g}^1 at around 385 cm⁻¹ and A_{1g} at 405 cm⁻¹, with a frequency difference of 20 cm⁻¹, typical of monolayer. A strong signal between 665 and 620 nm can be observed in the Photoluminescence spectra (figure 3(c)), which corresponds to A and B direct excitonic transitions. For Raman and Photoluminescence measurements, a confocal Raman spectrometer (WITec Alpha 300R) was utilized, incorporating a 100X objective lens and a 532 nm laser line with a laser power of 0.5 mW.

Back-gated field effect transistors were fabricated according to our previous work [16], using a 50 nm alumina (Al₂O₃) film as the gate oxide and a stack of Pt/TiN/p++Si as the back gate electrode. First, CVD-grown MoS₂ was transferred onto the alumina sample. The sample was spin-coated with A6 PMMA, followed by electron-beam (e-beam) lithography to specify the 2 μm channels, and then separated out by sulfur hexafluoride (SF₆) etch under 5 °C for 30 s. After each step, the sample was rinsed in acetone for 30 min, followed by a rinse in IPA. To define the source and drain contacts, the sample was spin-coated with methyl methacrylate (MMA) followed by A3 PMMA. The electron-beam lithography source and drain contacts were then patterned and further developed using a 1:1 mixture of 4-methyl-2-pentanone (MIBK) and IPA for 60 s. 40 nm of Ni and 30 nm of Au were deposited onto the patterns using electron beam (E-beam) evaporation. The evaporated materials were lifted off by immersing the sample in acetone for 30 min, followed by an IPA final rinse.

3. Results and discussion

Figure 4(a) displays in green the integrand in the right-hand side of equation (1) calculated over the whole spectrum, depicting the CA in red and the input signal in blue, both for the case of theoretically calculated DC conductivity for MoS₂. To isolate the effect of the presence of AuCl₃ coordinated complexes, every system in these calculations was subject to the same S vacancy concentration of 1%. Each CA was calculated over configurations containing a certain concentration of AuCl₃ from 0% to 1%. The red line in figure 4(a) represents one of these CAs, which was calculated over configurations containing 1% concentration of AuCl₃ impurity. The input function in blue has an unknown AuCl₃ concentration, to be determined via the inversion from the misfit depicted in green. Figure 4(b) shows the resulting misfit function, which has a very distinctive minimum indicating the impurity concentration that is likely to produce the smallest discrepancy when compared to the synthetic input signal. It is worth noting that the CA defined in equation (2) was calculated using only $N_c = 20$ configurations for seven different disorder concentration values n , seen on the horizontal axis. Given the large integration range of this particular inversion, a relatively low N_c number is enough to compute a high accuracy inversion considering the ergodic properties of the problem [26]. We, then, selected an arbitrary disorder concentration (in this case 0.5%, indicated by the vertical red dashed line) to characterize our synthetically generated input function $\Gamma(E)$ and compared it with the previously obtained CAs calculated via

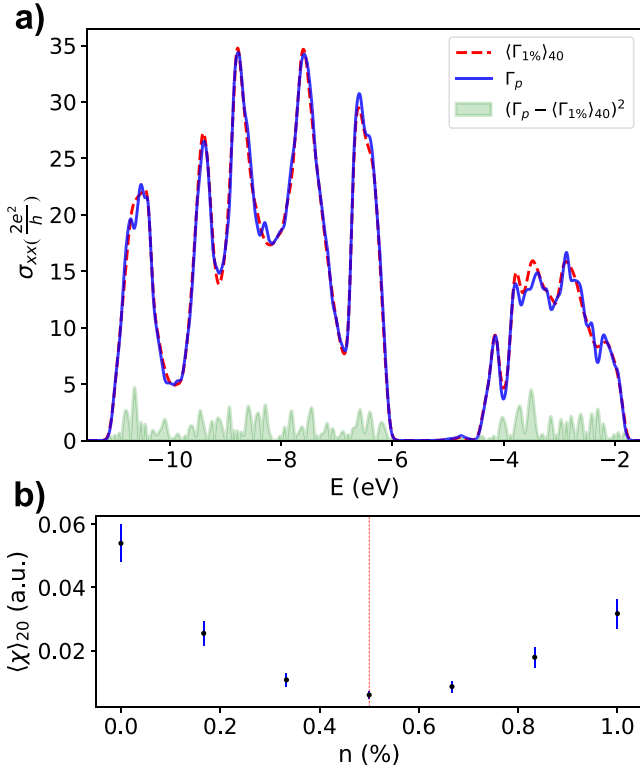


Figure 4. (a) Longitudinal DC conductivity at temperature $T = 300$ K comparison (filled green region) between 1% AuCl_3 concentration CA (dashed red line) and input configuration signal (solid blue line) containing unknown AuCl_3 concentration. The CA is composed of 40 configurations and all systems have a 1% concentration of S vacancies. (b) Misfit function $\chi(n)$ in arbitrary units averaged over 20 distinct inversion instances with minima at 0.5% AuCl_3 concentration. The vertical (red) line indicates the real concentration of the input configurations.

equation (1). Repeating this procedure for multiple input functions with the same disorder concentration, we generate the average misfit values and respective standard deviations indicated by the error bars around the data points. The presence of such a clear minimum that coincides with the red line indicates that the inversion was successful. Furthermore, from the minimum relative depth and the respective standard deviations, we can conclude that the inversion was not only successful but also very accurate.

Remarkably, this result reveals that this inversion methodology is indeed capable of resolving the contribution of a minute concentration of adsorbed atoms and molecules to the DC conductivity of a disordered structure, even when such complexes weakly affect the charge mobility signature of the system [16]. This configures an expansion of the method's applicability now encompassing a new type of complex disorder, also testifying to its general accuracy and robustness.

To demonstrate that this method has a practical use beyond the case of synthetically generated Hamiltonians, it remains to prove that the inversion can be carried out from realistic experimental data. To answer this question resourcefully, we can approach the same inversion problem with a different lens—instead of determining the concentration of disorder for

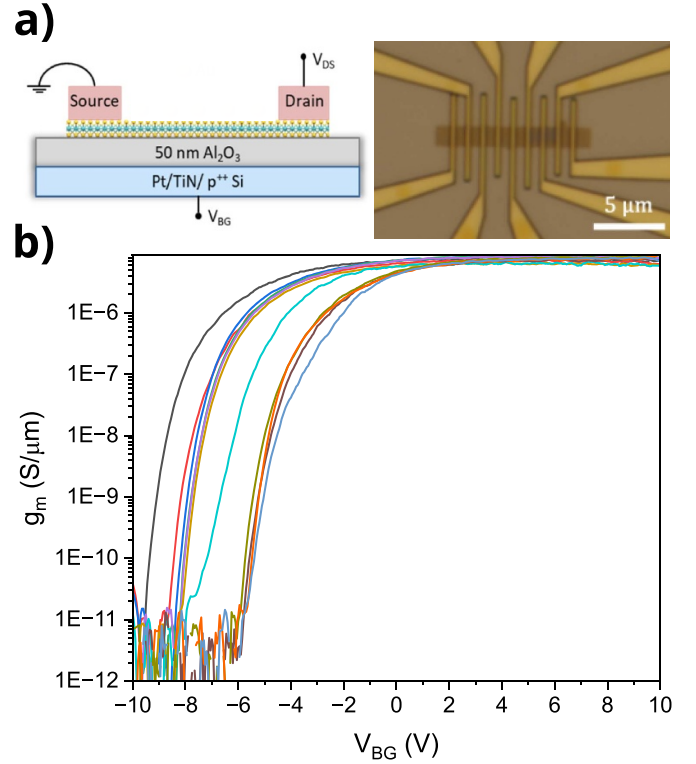


Figure 5. MoS_2 BGFET devices (a) Schematic of a back-gated field effect transistor on the MoS_2 channel and optical image of the fabricated devices showing the lateral structure. (b) Transconductance ($g_m = dI_{DS}/dV_{BG}$) vs back-gate voltage (V_{BG}) with a drain bias of 1 V for 12 different pristine MoS_2 BGFETs.

designing a material with certain properties, we can attempt to decode the impurity concentration in a sample by using its experimental signal as the input function $\Gamma(E)$. It is then useful to simplify the system to mono-layer MoS_2 containing vacancies as the only source of disorder due to the current data availability. Verily, chalcogen vacancies in the MoS_2 are one of the most common types of defects that occur during fabrication, along with antisite or atomic defects depending on the sample preparation method [40]. This implies that for any attempt to design TMDs by engineering a specific defect concentration, it is very likely that the effect of vacancies will also be present. The presence of vacancies is also effective in unlocking properties on MoS_2 such as the introduction of a local magnetic moment, as well as the conversion of the compound into p- or n-type semiconductors [56, 57]. Therefore, the ability to identify vacancy concentrations in MoS_2 samples becomes exceptionally valuable. In previous work, we successfully performed an inversion of MoS_2 containing chalcogen vacancies from theoretically calculated input signals [26]. In the following result, we present an experimental counterpart of that inversion.

Twelve back-gated field effect transistors (BGFETs) were designed and fabricated, according to our previous work [16] (figure 5), to extract the drain current (I_{DS}) versus the back gate voltage (V_{BG}). The transconductance (g_m) versus V_{BG} , defined as $g_m = dI_{DS}/dV_{BG}$, was used as input function $\Gamma(E)$ to calculate the vacancy concentration on the MoS_2 flakes.

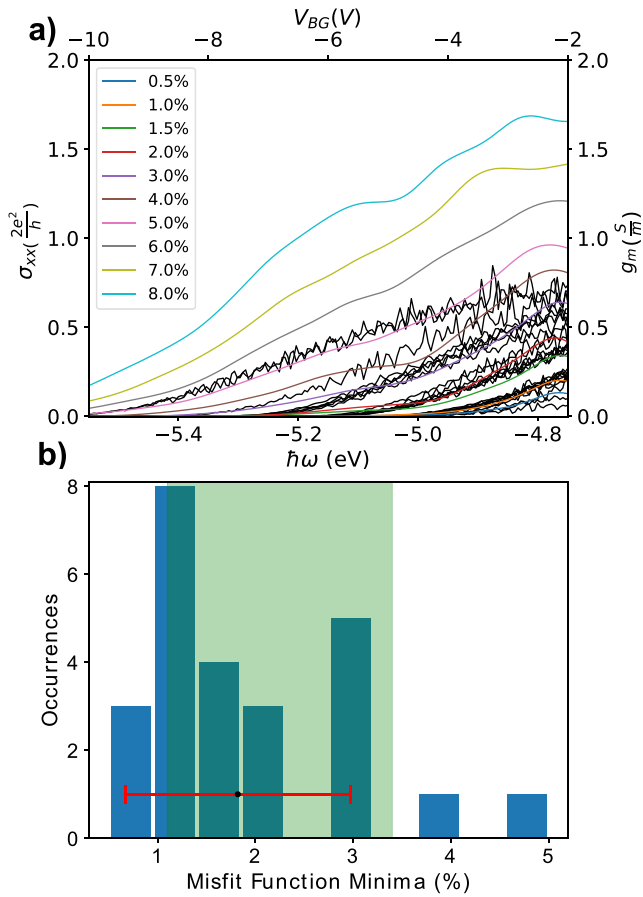


Figure 6. (a) Comparison between simulated MoS₂ DC conductivity at $T = 300$ K containing different vacancy concentrations (colored) and experimental conductivity data— g_m values normalized by the ratio between the gate width and length—for various MoS₂ systems (black), each of which contains unknown vacancy concentration. (b) Histogram of the minima of the different misfit functions for each black curve of (a). The black dot and red bar indicate the Gaussian mean and standard deviation of the minima distribution at $1.8 \pm 1.1\%$. The area in green represents the expected range of vacancy concentration previously reported for this method of fabrication.

Figure 5(b) shows $g_m \times V_{BG}$ curves of representatives of the twelve pristine MoS₂ BGFET. The observed threshold voltage (V_T) variation, between -10 and -5 V, can be attributed to different defect densities on the MoS₂ flake affecting the Fermi energy and electron mobility. The calculated average field effect mobility (μ_{FE}) was 15 ± 10 cm²/V^{-s}, which is comparable to the mobility values reported for exfoliated single crystal material [58]. The ON state current was found to be approximately $120 \mu\text{A } \mu\text{m}^{-1}$ at $V_{DS} = 8$ V and $V_{BG} = 10$ V. The calculated subthreshold slope (SS) was 350 mV/decade.

Using the parametrization adopted in the earlier DFT calculations for the pristine mono-layer MoS₂, we can introduce chalcogen vacancies through KITE’s environment. Performing calculations with similar parameters as the ones discussed previously, we arrive at CAs for MoS₂ at various vacancy concentrations. Figure 6(a) presents the experimental transconductivity data (black) and

the calculated CAs conductivity in colored curves, establishing a visual comparison that highlights the effect of vacancies on the conductivity curves and the possible concentration of vacancies present in the experimental data. Assuming the system is composed of pure MoS₂ and S vacancies, we can invert the experimental data to obtain the misfit functions minima as presented in figure 6(b). Through the inversions, we find vacancy concentrations falling within and around the expected range of 1.2%–3.4% of vacancy concentrations for CVD-grown MoS₂ [40, 59, 60].

The direct application of the presented method on an input signal generated from experimental data closes the gap between inversion tools being potentially useful and being of practical utility. Furthermore, it establishes that tools of that type can be employed as a reliable mechanism for material design and characterization.

4. Conclusion

In conclusion, we tackled two fronts of the presented inversion method application. We established that the method can be combined with first-principles calculations to perform complex, more realistic simulations and that its robustness and accuracy are preserved even when dealing with scatterers which possess extremely weak and feeble signatures.

This study also pioneered the method’s implementation along with experimental data, where it displayed clear compatibility, paving its way for realistic applications in characterization and material design. To complement the results presented in the experimental-signal inversion part of this work, a systematic characterization of the material samples quantifying the different types of disorder present in the system will allow for a quantitative evaluation of the method’s accuracy. It is also important to emphasize that, in cases where the inverted function is subject to impurities with extremely weak signatures, the accuracy of the method relies on the precision and resolution of the input function. If one would attempt an inversion of an experimental signal containing AuCl₃ complexes, for example, the conductivity experimental measurements must be correspondingly sensitive to the characteristic signatures of this type of disorder. At this higher level of precision not only the characterization of disorder concentration of AuCl₃ is needed to evaluate the method’s accuracy, but also characterizations of the other possible impurities that may have stronger signatures, such as vacancies.

Finally, given the growing interest in material design and the demonstration that inversion methodologies do play a significant role in our capacity to engineer the physical properties of materials, it is encouraging to see that such tools are becoming more reliable, even in the presence of disorder. This is an important step towards the goal of reducing the computational complexity that is involved in the search for new materials and, in a period when contemporary material design research is greatly driven by machine learning algorithms, this work offers a transparency that is essential for the overall understanding of the research area, in contrast to full black-box approaches.

Data availability statement

All data that support the findings of this study are included within the article (and any supplementary files).

Acknowledgments

This publication has emanated from research supported in part by a research grant from Science Foundation Ireland (SFI) under Grant No. **SFI12RC2278_P2**. F R D wishes to acknowledge the Irish Centre for High-End Computing (ICHEC) and Trinity Centre for High-Performance Computing (Research IT) for the provision of computational facilities and support. C J S d M and D G acknowledge financial support from FAPESP (Grant Nos. 2015/10405-3, 2017/01817-1 and 2018/07276-5), FINEP (Grant No. 01.22.0208.00), and the Brazilian Nanocarbon Institute of Science and Technology (INCT/Nanocarbon). L S acknowledges financial support from FAPESP (Grant No. 2022/14549-3) and the National Institute of Science and Technology on Materials Informatics (INCT/Materials Informatics, Grant No. 371610/2023-0). C J S d M and L S acknowledge financial support from CAPES-PrInt (Grant No. 88887.310281/2018-00). D G acknowledges financial support from Rio de Janeiro State Foundation (FAPERJ—Grant Nos. E-26/210.296/2022, E-26/201.254/2022 and E-26/211.464/2021) and Serrapilheira Institute (Grant Number R-2012-37959).

Author contributions

FRD co-wrote the paper and conducted all the spectral simulations and data analysis. FM conducted the TB parametrization from DFT data and co-wrote the paper. DG conducted the experimental part and co-wrote the paper. LS conducted the DFT calculations. ARR led the TB parametrization. SM aided the theoretical implementations. CJSdM co-led the experimental part of the research. MSF led the research. All authors discussed and commented on the manuscript and on the results.

Conflict of interest

The authors declare no Competing Financial or Non-Financial Interests.

KITE

KITE has an open-access repository at <https://zenodo.org/record/3245011> and <https://quantum-kite.com/>.

ORCID iDs

F R Duarte  <https://orcid.org/0000-0003-3065-4454>
 F Matusalem  <https://orcid.org/0000-0002-5305-9693>
 D Grasseschi  <https://orcid.org/0000-0001-6066-0869>
 A R Rocha  <https://orcid.org/0000-0001-8874-6947>

Leandro Seixas  <https://orcid.org/0000-0001-7420-0708>
 S Mukim  <https://orcid.org/0000-0002-5475-5551>
 M S Ferreira  <https://orcid.org/0000-0002-0856-9811>

References

- [1] Huang H H, Fan X, Singh D J and Zheng W T 2020 Recent progress of TMD nanomaterials: phase transitions and applications *Nanoscale* **12** 1247–68
- [2] Choi W, Choudhary N, Hee Han G, Park J, Akinwande D and Hee Lee Y 2017 Recent development of two-dimensional transition metal dichalcogenides and their applications *Mater. Today* **20** 116–30
- [3] Li Z, Meng X and Zhang Z 2018 Recent development on MoS₂-based photocatalysis: a review *J. Photochem. Photobiol. C* **35** 39–55
- [4] Li X and Zhu H 2015 Two-dimensional MoS₂: properties, preparation and applications *J. Mater.* **1** 33–44
- [5] Krishnan U, Kaur M, Singh K, Kumar M and Kumar A 2019 A synoptic review of MoS₂: synthesis to applications *Superlattices Microstruct.* **128** 274–97
- [6] Vancsó P, Hagymási I, Castenetto P and Lambin P 2019 Stability of edge magnetism against disorder in zigzag MoS₂ nanoribbons *Phys. Rev. Mater.* **3** 094003
- [7] Nieminen J, Dhara S, Chiu W-C, Mucciolo E R and Bansil A 2023 Atomistic modeling of a superconductor–transition metal dichalcogenide–superconductor Josephson junction *Phys. Rev. B* **107** 174524
- [8] Sohler T, de Melo P M M C, Zanolli Z and Jean Verstraete M 2023 The impact of valley profile on the mobility and Kerr rotation of transition metal dichalcogenides *2D Mater.* **10** 025006
- [9] Garcia J H, You J, García-Mota M, Koval P, Ordejón P, Cuadrado R, Verstraete M J, Zanolli Z and Roche S 2022 Electrical control of spin-polarized topological currents in monolayer WTe₂ *Phys. Rev. B* **106** L161410
- [10] Sun Z, Martinez A and Wang F 2016 Optical modulators with 2D layered materials *Nat. Photon.* **10** 227–38
- [11] Zheng W, Jiang Y, Hu X, Li H, Zeng Z, Wang X and Pan A 2018 Light emission properties of 2D transition metal dichalcogenides: fundamentals and applications *Adv. Opt. Mater.* **6** 1800420
- [12] Zhou W, Gong H, Jin X, Chen Y, Huimin Li and Liu S 2022 Recent progress of two-dimensional transition metal dichalcogenides for thermoelectric applications *Front. Phys.* **10** 67
- [13] Chou S S, De M, Kim J, Byun S, Dykstra C, Yu J, Huang J and Dravid V P 2013 Ligand conjugation of chemically exfoliated MoS₂ *J. Am. Chem. Soc.* **135** 4584–7
- [14] Ding Q, Czech K J, Zhao Y, Zhai J, Hamers R J, Wright J C and Jin S 2017 Basal-plane ligand functionalization on semiconducting 2H-MoS₂ monolayers *ACS Appl. Mater. Interfaces* **9** 12734–42
- [15] Mouri S, Miyauchi Y and Matsuda K 2013 Tunable photoluminescence of monolayer MoS₂ via chemical doping *Nano Lett.* **13** 5944–8
- [16] Liu H et al 2020 Spontaneous chemical functionalization via coordination of Au single atoms on monolayer MoS₂ *Sci. Adv.* **6** eabc9308
- [17] Voiry D, Yang J and Chhowalla M 2016 Recent strategies for improving the catalytic activity of 2D TMD nanosheets toward the hydrogen evolution reaction *Adv. Mater.* **28** 6197–206
- [18] Lin L, Sherrell P, Liu Y, Lei W, Zhang S, Zhang H, Wallace G G and Chen J 2020 Engineered 2D transition metal dichalcogenides—a vision of viable hydrogen evolution reaction catalysis *Adv. Energy Mater.* **10** 1903870

- [19] Yarali M, Brahmi H, Yan Z, Li X, Xie L, Chen S, Kumar S, Yoon M, Xiao K and Mavrokefalos A 2018 Effect of metal doping and vacancies on the thermal conductivity of monolayer molybdenum diselenide *ACS Appl. Mater. Interfaces* **10** 4921–8
- [20] Wang S, Robertson A and Warner J H 2018 Atomic structure of defects and dopants in 2D layered transition metal dichalcogenides *Chem. Soc. Rev.* **47** 6764–94
- [21] Chen X and McDonald A R 2016 Functionalization of two-dimensional transition-metal dichalcogenides *Adv. Mater.* **28** 5738–46
- [22] Presolski S and Pumera M 2016 Covalent functionalization of MoS₂ *Mater. Today* **19** 140–5
- [23] Suh J *et al* 2014 Doping against the native propensity of MoS₂: degenerate hole doping by cation substitution *Nano Lett.* **14** 6976–82
- [24] Mukherjee R, Chuang H J, Koehler M R, Combs N, Patchen A, Zhou Z X and Mandrus D 2017 Substitutional electron and hole doping of WSe₂: synthesis, electrical characterization and observation of band-to-band tunneling *Phys. Rev. Appl.* **7** 034011
- [25] Mukim S, Amorim F P, Rocha A R, Muniz R B, Lewenkopf C and Ferreira M S 2020 Disorder information from conductance: a quantum inverse problem *Phys. Rev. B* **102** 075409
- [26] Duarte F R, Mukim S, Molina-Sánchez A, Rappoport T G and Ferreira M S 2021 Decoding the DC and optical conductivities of disordered MoS₂ films: an inverse problem *New J. Phys.* **23** 073035
- [27] Mukim S, Lewenkopf C and Ferreira M S 2022 Spatial mapping of disordered 2D systems: the conductance Sudoku *Carbon* **188** 360–6
- [28] Mukim S, O'Brien J, Abarashi M, Ferreira M S and Rocha C G 2021 Decoding the conductance of disordered nanostructures: a quantum inverse problem *J. Phys.: Condens. Matter* **34** 085901
- [29] Ries L *et al* 2019 Enhanced sieving from exfoliated MoS₂ membranes via covalent functionalization *Nat. Mater.* **18** 1112–7
- [30] Voiry D, Goswami A, Kappera R, de Carvalho Castro e Silva C, Kaplan D, Fujita T, Chen M, Asefa T and Chhowalla M 2015 Covalent functionalization of monolayered transition metal dichalcogenides by phase engineering *Nat. Chem.* **7** 45–49
- [31] Knirsch K C *et al* 2015 Basal-plane functionalization of chemically exfoliated molybdenum disulfide by diazonium salts *ACS Nano* **9** 6018–30
- [32] Cysne T P, Rappoport T G, Ferreira A, Viana Parente Lopes J M and Peres N M R 2016 Numerical calculation of the Casimir-Polder interaction between a graphene sheet with vacancies and an atom *Phys. Rev. B* **94** 235405
- [33] João S M and Viana Parente Lopes J M 2019 Basis-independent spectral methods for non-linear optical response in arbitrary tight-binding models *J. Phys.: Condens. Matter* **32** 125901
- [34] Jung J and MacDonald A H 2014 Accurate tight-binding models for the π bands of bilayer graphene *Phys. Rev. B* **89** 035405
- [35] Garcia-Fernandez P, Wojdeł J C, Iniguez J and Junquera J 2016 Second-principles method for materials simulations including electron and lattice degrees of freedom *Phys. Rev. B* **93** 195137
- [36] Liang Q, Zhang Q, Zhao X, Liu M and Wee A T S 2021 Defect engineering of two-dimensional transition-metal dichalcogenides: applications, challenges and opportunities *ACS Nano* **15** 2165–81
- [37] Guo Y, Liu D and Robertson J J A P L 2015 Chalcogen vacancies in monolayer transition metal dichalcogenides and Fermi level pinning at contacts *Appl. Phys. Lett.* **106** 173106
- [38] Mitterreiter E *et al* 2021 The role of chalcogen vacancies for atomic defect emission in MoS₂ *Nat. Commun.* **12** 3822
- [39] Zhou W, Zou X, Najmaei S, Liu Z, Shi Y, Kong J, Lou J, Ajayan P M, Yakobson B I and Idrobo J-C 2013 Intrinsic structural defects in monolayer molybdenum disulfide *Nano Lett.* **13** 2615–22
- [40] Hong J *et al* 2015 Exploring atomic defects in molybdenum disulphide monolayers *Nat. Commun.* **6** 6293
- [41] Matusalem F, Marques M, Teles L K and Bechstedt F 2015 Stability and electronic structure of two-dimensional allotropes of group-IV materials *Phys. Rev. B* **92** 045436
- [42] Soler J M, Artacho E, Gale J D, García A, Junquera J, Ordejón P and Sánchez-Portal D 2002 The SIESTA method for ab initio order-N materials simulation *J. Phys.: Condens. Matter* **14** 2745–79
- [43] Murray E D, Lee K and Langreth D C 2009 Investigation of exchange energy density functional accuracy for interacting molecules *J. Chem. Theory Comput.* **5** 2754–62
- [44] Perdew J P, Burke K and Ernzerhof M 1996 Generalized gradient approximation made simple *Phys. Rev. Lett.* **77** 3865–8
- [45] Vydrov O A and Van Voorhis T 2010 Nonlocal van der Waals density functional: the simpler the better *J. Chem. Phys.* **133** 244103
- [46] Bertel R, Mora-Ramos M E and Correa J D 2022 Effects of van der Waals interaction on the adsorption of H₂ on MoS₂ monolayers and nanoribbons *Chem. Phys.* **555** 111446
- [47] Marzari N and Vanderbilt D 1997 Maximally localized generalized Wannier functions for composite energy bands *Phys. Rev. B* **56** 12847–65
- [48] Souza I, Marzari N and Vanderbilt D 2002 Maximally localized Wannier functions for entangled energy bands *Phys. Rev. B* **65** 1–13
- [49] Pizzi G *et al* 2020 Wannier90 as a community code: new features and applications *J. Phys.: Condens. Matter* **32** 165902
- [50] Molina-Sánchez A, Sangalli D, Hummer K, Marini A and Wirtz L 2013 Effect of spin-orbit interaction on the optical spectra of single-layer, double-layer and bulk MoS₂ *Phys. Rev. B* **88** 045412
- [51] Hüser F, Olsen T and Thygesen K S 2013 How dielectric screening in two-dimensional crystals affects the convergence of excited-state calculations: monolayer MoS₂ *Phys. Rev. B* **88** 1–9
- [52] João S M, Andelković M, Covaci L, Rappoport T G, Lopes J ao M V P and Ferreira A 2020 KITE: high-performance accurate modelling of electronic structure and response functions of large molecules, disordered crystals and heterostructures *R. Soc. Open Sci.* **7** 191809
- [53] João S ao M, Viana Parente Lopes J M and Ferreira A 2022 High-resolution real-space evaluation of the self-energy operator of disordered lattices: Gade singularity, spin-orbit effects and p-wave superconductivity *J. Phys. Mater.* **5** 045002
- [54] Veiga H P, João S M, Pinho J M, Pires J P and Lopes J M 2023 Unambiguous simulation of diffusive charge transport in disordered nanoribbons (arXiv:2311.03983)
- [55] Depending on the desired spectral range of interest, we can further improve the accuracy of the conductivity calculations by implementing a single-shot energy approach [52] on even larger systems with the cost of having only one energy value calculated at a time
- [56] Zhou Y, Yang P, Zu H, Gao F and Zu X 2013 Electronic structures and magnetic properties of MoS₂ nanostructures:

- atomic defects, nanoholes, nanodots and antidots *Phys. Chem. Chem. Phys.* **15** 10385–94
- [57] Yang D, Fan X, Zhang F, Hu Y and Luo Z 2019 Electronic and magnetic properties of defected monolayer WSe₂ with vacancies *Nanoscale Res. Lett.* **14** 1–9
- [58] Schulman D S, Arnold A J and Das S 2018 Contact engineering for 2D materials and devices *Chem. Soc. Rev.* **47** 3037–58
- [59] Manoj Gali S, Pershin A, Lherbier A, Charlier J-C and Beljonne D 2020 Electronic and transport properties in defective MoS₂: impact of sulfur vacancies *J. Phys. Chem. C* **124** 15076–84
- [60] Roy S, Choi W, Jeon S, Kim D-H, Kim H, Joon Yun S, Lee Y, Lee J, Kim Y-M and Kim J 2018 Atomic observation of filling vacancies in monolayer transition metal sulfides by chemically sourced sulfur atoms *Nano Lett.* **18** 4523–30